FEATURE ARTICLE

Molecular Orientation at Surfaces: Surface Roughness Contributions to Measurements Based on Linear Dichroism

Garth J. Simpson and Kathy L. Rowlen*

Department of Chemistry and Biochemistry, University of Colorado, Boulder, Colorado 80309

Received: September 30, 1998; In Final Form: December 18, 1998

The molecular orientation at surfaces plays a key role in many of the interesting optical properties of organic thin films. Accurate determination of molecular "tilt" angles and the distribution in tilt angles is essential for an improved understanding of performance characteristics, i.e., the structure−function relationship. While there are several spectroscopic techniques available for measurement of molecular orientation at solid surfaces, little effort has been dedicated to understanding the contributions of surface roughness on measured orientation values. In this paper, following an overview of spectroscopic techniques and previous approximations of surface roughness effects, a quantitative theory for treating surface roughness contributions to molecular orientation measurements made by linear dichroism is presented. The theory is sufficiently general that it may be extended to other spectroscopic techniques, such as second-harmonic generation. It is anticipated that knowledge of the molecular orientation with respect to the local surface (i.e., accounting for surface roughness) will provide a better understanding of the orientation in organic thin films.

Introduction/Background

Measurement of the molecular orientation at surfaces and interfaces can provide valuable insights into the nature and structure of surface systems. The orientation of surface molecules has been used to characterize two-dimensional phase transitions,[1] the structure of monolayer and multilayer films,[2] and the structure of interfaces.[3] Orientation is also a key parameter in construction of practical devices based on self-assembly technology, including thin films for use in nonlinear optics,[4,5] as well as piezoelectric and pyroelectric detectors[6] and chemical sensors.[6] The most commonly used spectroscopic methods for determining the orientation of molecules at surfaces include fluorescence[7−9] and fluorescence depolarization,[10,11] linear dichroism (LD) using polarized infrared[12,13] and UV−vis light,[7,14−16] second-harmonic generation (SHG),[17−19] and sum-frequency generation (SFG).[20−22]

Motivation: The Surface Roughness Factor. The molecular orientation in a uniaxial system is determined by any of the above-mentioned spectroscopic techniques is "macroscopic" in nature and a measure of the net orientation defined with respect to a unique lab axis (typically the *Z*-axis). While this macroscopic measurement is indicative of the macroscopic optical properties, it does not necessarily take into account the local interaction between the molecule and the surface. For an atomically flat surface, the macroscopic molecular orientation is a true measure of the molecule's orientation with respect to the surface. However, for a noncrystalline rough surface, such as glass, the "local" surface can be tilted at an angle with respect to the macroscopic surface normal. In this case, a distribution in local surface tilt (or slope) can affect the net orientation of the molecule with respect to the macroscopic surface normal. While some effort has been made to *estimate* surface roughness contributions to orientation angles determined by the spectroscopic techniques mentioned above, to date there has been no quantitative theory for treating surface roughness contributions.

Text Organization. After a brief, comparative review of the most relevant spectroscopic techniques used for molecular orientation measurements, an overview of what is known about the influence of surface roughness is given. The theory section contains a concise review of terminology for linear dichroism and a general model for the separation of linear dichroism results into contributions attributable to local molecular orientation and to surface roughness. Specifically, a quantitative theory for treating the surface roughness contribution to molecular orientation measurements made by linear dichroism is given. In the Results and Discussion section, the theory's effectiveness is demonstrated by comparison with experimental results. The summary contains possible future applications and directions of the general approach.

Review of Spectroscopic Techniques: Fluorescence. In fluorescence measurements, the polarization of emitted light is typically used to determine the orientation of the emitting dipole and from that the molecular orientation.[7−9] Fluorescence depolarization techniques supplement standard fluorescence measurements by including time-domain information for different polarizations.[10,11] Since two photons are involved in fluorescence techniques (one absorbed and one emitted), it is sometimes possible to determine two order parameters describing the molecular orientation (e.g., the mean tilt angle and the spread about the mean). Additionally, fluorescence detection is highly sensitive, with submonolayer detection limits. One potential drawback of fluorescence techniques is that the molecule under

* To whom correspondence should be addressed.

10.1021/jp983912k CCC: $18.00 © 1999 American Chemical Society
Published on Web 04/08/1999

investigation must be reasonably fluorescent. Furthermore, polarized fluorescence intensities can be influenced by changes in fluorescence quantum yields induced by interactions with a surface.[23−26]

Nonlinear Techniques. SHG and SFG are nonlinear optical processes which are symmetry forbidden in bulk isotropic media and therefore selective for the interface between such media. Molecular orientation determination by SHG or SFG is achieved by relating the nonlinear optical properties of surface-constrained molecules to the macroscopic nonlinear optical response of the ensemble. From the polarized intensities of the nonlinearly generated light as a function of varying incident polarizations, the orientation of the molecular axis (or axes) responsible for the nonlinear response can be determined. SHG and SFG experiments have the distinct advantage of being applicable at buried interfaces and at interfaces in which bulk contributions preclude the use of fluorescence or absorbance techniques. However, quantitative correlation between the experimentally observed nonlinear response and molecular orientation can often be a complicated process.[19,27]

Linear Dichroism. In both infrared and visible absorption experiments, linear dichroism is measured from the ratio of absorbance for typically two (e.g., s and p) linear polarizations of incident light. For nonisotropic samples, the ratio in absorbance for the two excitation polarizations allows for the calculation of the average orientation of the transition dipole and from that the molecular orientation.[12−16] While linear dichroism measurements offer the distinct advantages of simplicity and near universality, traditional experimental configurations are generally limited to analysis of complete monolayer or multilayer surface films.

Angle-Resolved Photoacoustic Spectroscopy. ARPAS is a linear dichroism technique which relies on the acoustic signal generated when excited-state molecules decay nonradiatively. By varying the incident angle of plane-polarized light from a pulsed laser source with respect to the surface upon which molecules have been deposited, it is possible to extract the mean tilt angle of the surface-constrained molecules with respect to the lab *z*-axis, or surface normal. For example, for molecules uniaxially aligned along the surface normal and a transition dipole aligned along the molecular long axis (assumed here to be the principle orientation axis), the absorbance should increase as the electric field vector is rotated from parallel to perpendicular to the surface plane. Conversely, a transition dipole aligned perpendicular to the molecular long axis in the example just given would exhibit a decreasing signal.

Generation of excited states with pulsed excitation and subsequent nonradiative decay results in an acoustic wave. The amplitude of a photoinduced acoustic wave is proportional to the amount of energy absorbed; thus, below saturation, the signal can be enhanced by increasing the excitation beam intensity. Since the amplitude of the acoustic wave is proportional to both the intensity of excitation and sample absorbance, photoacoustic spectroscopy offers the combined advantages of sensitivity equivalent to that of fluorescence and the near universal utility and simplicity of absorbance detection. In addition, since the photoacoustic signal depends only on the amount of light absorbed, it is insensitive to scattered light, which can be troublesome in other spectroscopic techniques.

The reliability of ARPAS for molecular orientation measurements was demonstrated by comparing average orientation or "tilt" angles obtained by ARPAS with those obtained by other techniques for two separate molecular systems.[28] Specifically, the orientation of 1,4-bis(2-methylstyryl)benzene, partitioned into a chromatographic alkyl phase, was investigated as a function of solvent overlayer. ARPAS yielded approximately the same average angles of orientation as previously determined by fluorescence anisotropy.[29,30] The orientation of dimethylphenylsilane covalently bound to quartz was also investigated. A value of 71° ± 3° with respect to the surface normal was obtained for the transition centered near 260 nm, in agreement with previous studies.[31,32] In more recent work, ARPAS was used to probe the orientation of an azo dye chromophore in zirconium phosphate−phosphonate ($Zr-PO_x$) interlayers as a function of number of layers.[33] Figure 1 shows the trends in signal amplitude versus electric field angle as a function of the number of layers deposited. The average molecular tilt angle for the chromophore as a function of film thickness will be discussed in detail later in the text. However, it is important to note that independent of the mathematical function used to fit the data, there is a clear trend in the angular response and, therefore, in the average tilt angle. We believe that this study represented the first *direct* observation of a change in the orientation of a chromophore with the number of layers deposited using $Zr-PO_x$ interlayer chemistry.

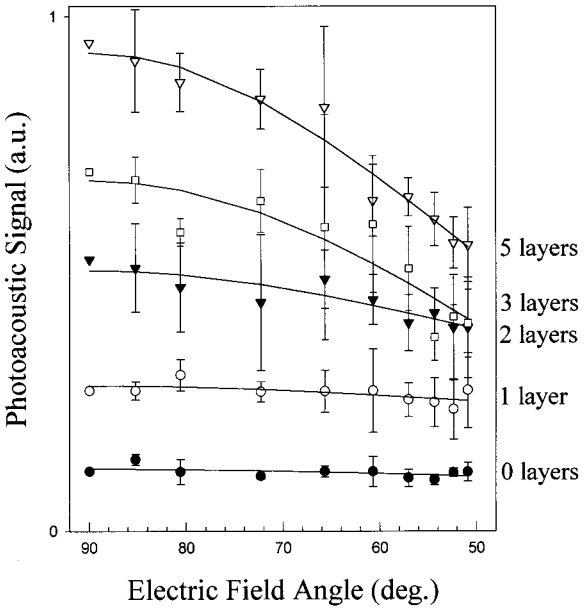

Figure 1. Representative ARPAS data for azo-dye $Zr-PO_x$ multilayer films as a function of the electric field angle of an excitation beam (reprinted from ref 33). The solid lines are nonlinear fits to the data. Details regarding data acquisition and the fitting procedure are described in detail in ref 33. As the number of layers was increased, the dependence of the ARPAS amplitude on the electric field angle changed, indicating a change in molecular orientation.

Overview of Substrate Roughness. Since silica surfaces are so widely used in spectroscopic studies of mono- and multilayers (for example, refs 28 and 33), this section focuses on the roughness of typical silica substrates. In a recent atomic force microscopic (AFM) investigation of fused silica "flats", we found the root-mean-square vertical displacement (or root-mean-square roughness, R_q) to be highly scan-size dependent, with R_q values greater than 13 Å observed at micrometer scan sizes.[34] Such R_q values attract interest since the magnitude is comparable to the thickness of a typical monolayer film (∼20−25 Å).

Precedent for surface roughness potentially influencing orientation measurements can be found by noting several examples where its effects have been at least qualitatively considered, including contact angles,[35,36] fluorescence[37,38] and fluorescence depolarization,[39−42] attenuated total internal reflection infrared spectroscopy,[6,43] electrochemical blocking,[44,45]

neutron[46−48] and X-ray[49−51] reflectivity, X-ray fluorescence,[52,53] and ellispometry.[54] As one example, in neutron reflectivity studies, Li et al.[48] and Lu et al.[46,47] demonstrated that amphiphile orientation at air−liquid interfaces could only be properly determined after correcting for the interface roughness. Neutron reflectivity exhibits molecular spatial resolution, allowing for determination of both the thickness of an interfacial layer and the spread in layer thickness. The presence of surface inhomogeneity by thermally generated capillary waves led to an apparent increase in the monolayer thickness for amphiphiles spread at the air/water interface.

The influence of interface roughness on molecular orientation has also been considered in a series of fluorescence depolarization studies conducted by Piasecki and Wirth[39,40] and by Burbage and Wirth.[41,42] The local, static spread in molecular orientation attributable to microscale molecular interactions was isolated from the spread due to roughness by calculation of the interface roughness using capillary wave theory. In this manner, the researchers were able to investigate the local, static roughness attributable solely to the molecular interactions at silica/C18/sodium dodecyl sulfate (SDS)/water,[42] hexadecane/SDS/water,[41] and liquid alkane/water[40] interfaces. In earlier work by Burbage and Wirth, in which the interfacial roughness was dominated by the roughness of a solid surface (fused silica/C18 surface in contact with water and water/alcohol solutions) rather than by capillary waves,[39] R_q was determined by AFM. When R_q values from analysis of a small scan size (20 nm × 20 nm) were used to estimate the contributions of roughness to the measured angular distribution, the contribution was found to be small (∼10%). However, when R_q was determined from a larger scan size (400 nm × 400 nm), the contribution of surface roughness to the measured distribution in the molecular orientation was found to be significant. In other studies, Firestone et al.[55] considered the influence of roughness on the spectroscopically determined orientation of surface-bound proteins on fused silica. AFM micrographs revealed a surface R_q of ∼15 Å for 1 μm × 1 μm scan sizes of the bare silica surface. Firestone et al. concluded that since R_q was less than the dimensions of the protein investigated (∼25 Å × 35 Å × 45 Å), surface roughness could be neglected.

Theory

Linear Dichroism and Molecular Tilt Angles. Barring external forces, linear dichroism in thin surface films arises exclusively from anisotropic molecular orientation. The net orientation of transition moment dipoles results in a polarization dependence on absorption. For a single transition moment in a single molecule, the probability for absorption scales with the squared cosine of the angle between the electric field vector and the transition moment axis, *f*. For an ensemble of absorbers, the squared cosine of the angle must be replaced with the ensemble average, or expectation value. Specifically, the absorbance for light polarized along an arbitrary lab axis, *U*, is given by[56]

$$A_U = A_{\max}\langle\cos^2\theta_{fU}\rangle \tag{1}$$

where $A_{\max}$ is the absorbance which would be measured if every transition moment were oriented exactly parallel to the excitation polarization axis, *U* is one of the mutually orthogonal lab *X*, *Y*, and *Z* axes, with *Z* being the macroscopic surface normal, θ_{fU} is the angle between the transition moment axis, *f*, and the polarization axis, *U*, and the brackets indicate an expectation value. Since expectation values of squared cosines occur frequently in discussions of linear dichroism, they are denoted here by the letter *K*, with subscripts indicating the axes defining the angle (for example, $K_{fU} = \langle\cos^2\theta_{fU}\rangle$). By the definition of an expectation value, the value of K_{fU} can be determined by integration over the distribution function ($P(\theta_{fU})$) describing the probability of finding a particular value of θ_{fU} if that function is known:

$$K_{fU} = \int_0^{\pi} \cos^2\theta_{fU} P(\theta_{fU}) \mathrm{d}\theta_{fU} \tag{2}$$

If the sample is uniaxially oriented (with the *Z*-axis being the unique axis, paralleling the surface normal), then $A_X = A_Y$ and $K_{fX} = K_{fY}$. While a uniaxial distribution is not a necessary condition, or even a valid one in many cases (e.g., after dipping or rubbing of a Langmuir−Blodgett film), most self-assembled ultrathin films are described well by uniaxial treatments. Combining the relation $K_{fX} = K_{fY}$ with the law of cosines (which states that $K_{fX} + K_{fY} + K_{fZ} = 1$) yields:

$$K_{fX} = K_{fY} = \frac{1}{2}(1 - K_{fZ}) \tag{3}$$

In many cases, including some grazing angle and total internal reflection methods, the ratio of A_Z to A_Y may be determined experimentally and from that the value of K_{fZ}. However, measurement of A_Z is often not made directly, as it requires an incident angle of 0°. Rather absorbance is measured at two or more electric field angles with respect to the surface normal, either by varying the angle of incidence for parallel polarized light or by varying the plane of polarization for a fixed angle of incidence. For an electric field vector polarized at an angle α from the surface normal (and an incident beam oriented at an angle of $\alpha \pm \pi/2$ for light polarized in the plane of incidence), the angle-resolved absorbance is given by:[56]

$$A(\alpha) = A_Z \cos^2\alpha + A_Y \sin^2\alpha \tag{4}$$

Combining eqs 3 and 4, followed by simplification, yields eq 5.

$$A(\alpha) = (A_{\max}/2)[\sin^2\alpha - K_{fZ}(3\sin^2\alpha - 2)] \tag{5}$$

If the absorbance is measured at two or more angles of α, then the value of K_{fZ} may be determined.

From the value of K_{fZ}, it is possible to determine the molecular tilt angle under certain conditions. In the following discussion, uppercase Roman letters *X*, *Y*, and *Z* indicate axes referenced to the lab frame and lowercase Greek letters ξ, ψ, and ζ to the molecular frame. Assuming a flat surface and a transition moment, *f*, lying along the principle orientation axis of the molecule, ζ (the long molecular axis for rodlike molecules), then $\theta_{fZ} = \theta_{\zeta Z}$ and $K_{fZ} = K_{\zeta Z}$ (a complete, general treatment of the roughness effect for arbitrary internal transition moment orientations is provided in the Appendix). The molecular tilt angle can then be evaluated once an appropriate distribution function has been chosen. Provided that the molecular tilt angle distribution about the mean is narrow (i.e., provided that the distribution function may be approximated by a Kronicker δ function), the mean tilt angle of the molecular ζ axis with respect to the lab frame is given by

$$\theta_{\zeta Z}^* = \theta_{fZ}^* \cong \cos^{-1}[(K_{fZ})^{1/2}] \tag{6}$$

where $\theta_{\zeta Z}^*$ is the apparent angle between the molecular ζ axis and the lab *Z* axis (see Figure 2a) or in other words the apparent

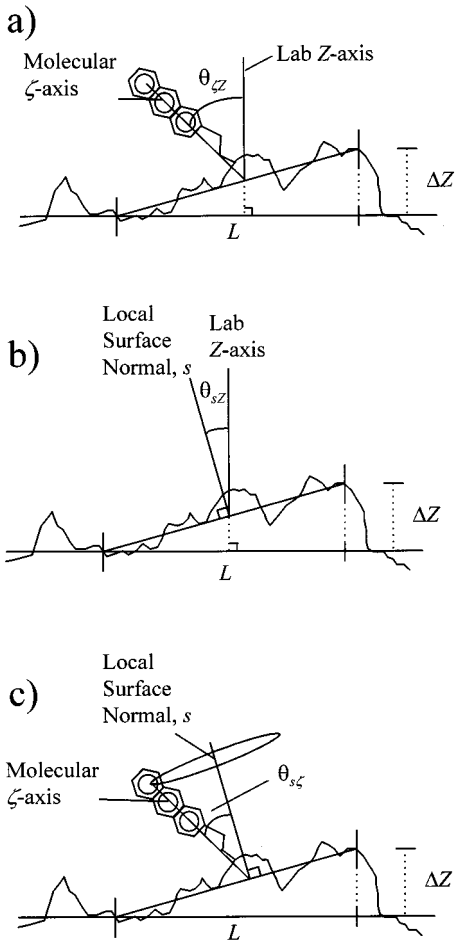

Figure 2. Schematic showing relevant angles in the treatment of roughness contributions to linear dichroism. (a) The macroscopic orientation angle, $\theta_{\zeta Z}$, is the angle between the lab *Z*-axis and the molecular ζ axis, with the ζ axis being the principle orientation axis of the surface-bound molecule. (b) The tilt angle of the local surface normal, θ_{sZ}, is a function of the cutoff length, *L*. Surface features smaller than *L* can be neglected (ref 57). In practice, the value of θ_{sZ} is determined from the surface gradient rather than the slope as shown. (c) The local molecular orientation angle, $\theta_{s\zeta}$, is defined by the angle between the local surface normal and the molecular ζ axis.

molecular tilt angle. The asterisk indicates that the angle is calculated assuming a δ-function distribution.

The molecular tilt angle defined in this manner is the value most often reported by linear dichroism investigations at surfaces. However, in the majority of such investigations, the approximation of a narrow distribution of tilt angles is unconfirmed since linear dichroism can only yield a single-order parameter describing the tilt angle distribution, typically the mean tilt angle. Other, independent, measurements of the distribution are necessary to gain more information.

Accounting for Substrate Roughness. If studies are conducted on a nonatomically flat substrate, surface roughness may influence the measured tilt angle distribution. As illustrated in Figure 2, if the "local" surface normal (*s*) (defined with respect to the length of the molecule) is not aligned with the macroscopic surface normal, the macroscopic distribution in molecular tilt angles will be affected by the distribution in the local surface tilt angle. In other words, the mean value of $\theta_{\zeta Z}$ is dependent on both the molecular tilt angle with respect to the local surface normal ($\theta_{s\zeta}$), and the tilt angle of the local surface normal (θ_{sZ}) due to roughness. In a previous study, we carefully examined the interrelationship between the cutoff length (*L*) used to calculate the local surface normal tilt (see Figure 2) and the values of θ_{sZ}, $\theta_{s\zeta}$, and $\theta_{\zeta Z}$.[57] It was demonstrated that the distribution in local molecular tilt angles is reasonably independent of the distribution in local surface tilt; therefore, the two functions are mathematically separable.

On the basis of the separability of the local molecular tilt angle and the local surface normal tilt angle, an expression for $K_{\zeta Z}$ can be derived in terms of expectation values related to each of the individual tilt angles. For a transition moment oriented parallel to the molecular ζ axis, a general expression for $K_{\zeta Z}$ is given by

$$K_{\zeta Z} = \langle \cos^2 \theta_{\zeta Z} \rangle = \langle (\sum_i \cos \theta_{s(z)i} \cos \theta_{s(i)Z})^2 \rangle \qquad (7)$$

where *i* refers to a molecular axis in the first cosine term (either ξ, ψ, or ζ) and a local surface axis in the second cosine term [either *s*(*x*), *s*(*y*), or *s*(*z*)]. The subscript *s(z)* denotes the axis containing the *local* surface normal, and *s(x)* and *s(y)* are orthogonal axes located in the *local* surface plane. Using both the orthogonality of the cosine functions and the separability of the local molecular and the local surface normal tilt angle distributions, the relation can be simplified to

$$K_{\zeta Z} = \sum_i \langle \cos^2 \theta_{s(z)i} \cos^2 \theta_{s(i)Z} \rangle = \sum_i \langle \cos^2 \theta_{s(z)i} \rangle \langle \cos^2 \theta_{s(i)Z} \rangle \qquad (8)$$

This derivation is based on a comparable treatment given in ref 56, in which the transition moment *f* is allowed to lie at an arbitrary internal angle away from the molecular orientation axis. Expansion of the sum leads to

$$K_{\zeta Z} = K_{s(z)\xi} K_{s(x)Z} + K_{s(z)\psi} K_{s(y)Z} + K_{s(z)\zeta} K_{s(z)Z} \qquad (9)$$

In each term of the sum, the first expectation value (e.g., $K_{s(z)\xi}$) is dependent only on the local molecular orientation and the second (e.g., $K_{s(x)Z}$) only on the surface tilt angle.

For a monolayer with uniaxial symmetry about the local surface normal (*s(z)*, see Figure 2c) and roughness features which are uniformly distributed in the surface plane, the distribution about the macroscopic surface normal is also uniaxial. Combining the uniaxial symmetries with the law of cosines yields the following two relations

$$K_{s(x)Z} = K_{s(y)Z} = \frac{1}{2}(1 - K_{s(z)Z}) \qquad (10)$$

$$K_{s(z)\xi} = K_{s(z)\psi} = \frac{1}{2}(1 - K_{s(z)\zeta}) \qquad (11)$$

which upon substitution into eq 9 yield

$$K_{\zeta Z} = \frac{1}{2}[1 - K_{sZ} - K_{s\zeta} + 3K_{sZ}K_{s\zeta}] \qquad (12)$$

where, for convenience, *s*, rather than *s(z)*, now refers to the axis containing the local surface normal.

The value of expressing $K_{\zeta Z}$ in the form given by eq 12 is immediately apparent. The macroscopic molecular tilt angle, $\theta_{\zeta Z}$, determined from linear dichroism measurements is expressed as a function of two independent expectation values, one of which (K_{sZ} or $\langle \cos^2 \theta_{sZ} \rangle$) is a function only of the substrate roughness and the other ($K_{s\zeta}$ or $\langle \cos^2 \theta_{s\zeta} \rangle$) only of the local molecular properties of the ultrathin film. Linear dichroism measurements alone can only yield information about the macroscopic tilt angle, which is a convolution of the "true" local

orientation and roughness effects. However, combining linear dichroism measurements with surface roughness measurements, as made by AFM, for example, provides a means to evaluate the local molecular orientation.

Case Analysis: The Extremes. Further insight to the physical significance of eq 12 can be gained by exploring the behavior of $K_{\zeta Z}$ in the limits of infinitely smooth and rough surfaces. For a perfectly smooth surface, θ_{sZ} will be a constant of 0, leading to a value of K_{sZ} equal to unity and a value of $K_{\zeta Z}$ equal to $K_{s\zeta}$. In other words, for a smooth surface with a transition moment parallel to the ζ axis, the tilt angle of the ζ axis with respect to the local surface normal is equal to its tilt angle with respect to the macroscopic surface normal, as expected. In the other extreme case of an infinitely rough surface, K_{sZ} will be equal to 1/3 (corresponding to the magic angle result of $\theta_{sZ} = 54.7°$ for an unoriented system),[57] leading to a value for $K_{\zeta Z}$ of 1/3 regardless of the local molecular tilt angle, $\theta_{s\zeta}$. In this case, the expectation value for the transition moment tilt angle is equal to that of an unoriented system regardless of the local molecular orientation. Conversely, if no orientation is present locally (i.e., the monolayer itself is unoriented), $K_{s\zeta}$ will equal 1/3, again leading to the expected value for $K_{\zeta Z}$ of 1/3 and a tilt angle $\theta_{\zeta Z}$ of 54.7°, regardless of the surface roughness.

Local Surface Orientation (Surface Tilt). There is no a priori reason that eq 12 could not be used to determine either K_{sZ} or $K_{s\zeta}$ from measurement of $K_{\zeta Z}$ provided that the other is known. However, surface roughness can be reasonably well characterized by one or more appropriate methods, while the local molecular orientation is more elusive and generally the parameter of interest. Therefore, it is desirable to be able to quantitatively predict the value of K_{sZ} from measurements of the surface roughness to isolate and evaluate $K_{s\zeta}$. As in eq 2, the value of K_{sZ} is given by

$$K_{sZ} = \langle \cos^2 \theta_{sZ} \rangle = \int_0^{\pi} \cos^2 \theta_{sZ} P(\theta_{sZ}) \mathrm{d}\theta_{sZ} \qquad (13)$$

where $P(\theta_{sZ})$ is the probability distribution function describing the likelihood of finding a particular local surface normal tilt angle, θ_{sZ}. In previous work, we have demonstrated that the distribution function $P(\theta_{sZ})$ for a surface with a Gaussian height distribution is accurately described by[57]

$$P_{2D}(\theta_{sZ}) = N_{2D} \theta_{sZ} \sec^2(\theta_{sZ}) \exp[-(L \tan \theta_{sZ})^2 / 2\sigma_{Z,\mathrm{eff}}^2] \qquad (14)$$

where P_{2D} is the two-dimensional probability of finding a particular local surface normal tilt angle (θ_{sZ}) within the surface plane, N_{2D} is a normalization constant, L is the cutoff length (dictated from the molecular length, see Figure 2), and $\sigma_{Z,\mathrm{eff}}$ is the effective surface roughness and is related to the root-mean-square roughness of the surface. In essence, $\sigma_{Z,\mathrm{eff}}$ is the root-mean-square height difference between two points on the surface separated by a specified distance (evaluation of $\sigma_{Z,\mathrm{eff}}$ from topographic measurements is discussed in detail in later sections). For a Gaussian height distribution, the probability of finding a particular difference in heights for a given lateral separation can be related to the probability of finding either a particular slope (in one surface dimension) or a particular gradient (in two surface dimensions).[57]

Case Analysis. In the limit of $\sigma_{Z,\mathrm{eff}} \ll L$ (such that $\tan^2 \theta_{sZ} \approx \theta_{sZ}^2 \approx (\Delta Z/L)^2$), the distribution in eq 14 can be approximated as

$$P_{2D}(\theta_{sZ}) \cong (1/\sigma_\theta^2) \theta_{sZ} \exp[-\theta_{sZ}^2 / 2\sigma_\theta^2] \qquad (15)$$

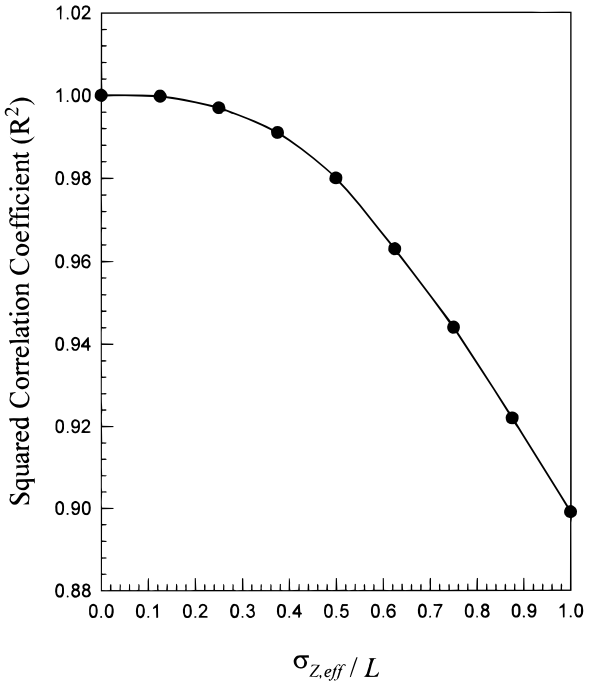

Figure 3. Evaluation of the approximated distribution (given by eq 15) as the effective roughness approaches the molecular size. The correlation coefficient was calculated from a comparison of the approximate distribution in eq 15 with the "true" distribution given by eq 14. Provided that $\sigma_{Z,\mathrm{eff}} \leq L/2$, the approximate distribution is reasonably accurate ($R^2 \leq 0.98$).

where $\sigma_\theta = \sigma_{Z,\mathrm{eff}}/L$. Equation 15 is a Gaussian distribution modified by a preexponential factor.

The physical basis for the probability distribution given in eq 14 is easiest to understand by examining the approximate distribution in eq 15. For a Gaussian height distribution, the distribution in tilts in one surface dimension will be approximately Gaussian as well, provided that $\tan^2 \theta_{sZ} \approx \theta_{sZ}^2 \approx (\Delta Z/L)^2$. Extending the distribution to include both surface dimensions simply involves multiplication of the one-dimensional Gaussian distribution by a geometric factor of $2\pi\theta_{sZ}$ (before normalization). This geometric term accounts for the fact that the tilt is a function of the surface *gradient* when both surface dimensions are considered and not of the slope measured along a single dimension. The factor of $2\pi\theta_{sZ}$ can be thought of as the effective "degeneracy" of finding a particular gradient, given a Gaussian probability along each surface dimension. An exactly analogous treatment can be found in the formulation of the two-dimensional Maxwell−Boltzmann distribution of speeds.[58]

The range of validity of the approximate distribution in eq 15 can be estimated by calculating the correlation coefficient between the "true" distribution (eq 14) and the approximate distribution (eq 15) as a function of the relative magnitude of the molecular size, shown in Figure 3. As a general guideline, reasonably accurate results are expected for most measurements using the approximate distribution in eq 15, provided that the effective roughness is less than about one-half of the molecular size ($R^2 \leq 0.98$ in Figure 3).

Approximate distributions similar to that described in eq 15 have been previously proposed by Piasicki and Wirth,[39,40] Wirth and Burbage,[41] and Burbage and Wirth[42] for treating the influence of roughness on fluorescence measurements at a variety of liquid surfaces and interfaces. In their work, the local surface normal tilt angle distribution was assumed to be Gaussian, with the effective roughness equal to the root-mean-square roughness calculated using capillary wave theory for a

cutoff length equal to the molecular size. The distribution in eq 15 differs most notably from the previously reported distributions by the preexponential factor of θ_{sZ} (which accounts for both surface dimensions) and the use of an effective roughness which incorporates both the surface topography and the fact that the slope is dependent on the height *difference* between points (as opposed to the displacement from the mean height).

With a functional form for the local surface normal tilt angle distribution, the surface tilt expectation value, K_{sZ}, in eq 13 can be evaluated by integration

$$K_{sZ} = N_{2D}\int_0^{\pi/2} \cos^2\theta_{sZ}\theta_{sZ}\sec^2(\theta_{sZ}) \times \exp[-(L\tan\theta_{sZ})^2/\sigma^2_{Z,\mathrm{eff}}]\mathrm{d}\theta_{sZ} \quad (16)$$

where the normalization constant is given by

$$N_{2D} \equiv \int_0^{\pi/2}\theta_{sZ}\sec^2(\theta_{sZ})\exp[-(L\tan\theta_{sZ})^2/\sigma^2_{Z,\mathrm{eff}}]\mathrm{d}\theta_{sZ} \quad (17)$$

In general, eqs 16 and 17 may be solved numerically. However, for relatively smooth surfaces (i.e., such that the condition $\sigma_{Z,\mathrm{eff}} \leq L/2$ described in Figure 3 is satisfied), the approximate distribution given by eq 15 is reasonably accurate and eq 17 may be simplified to

$$K_{sZ} \cong (1/\sigma^2_\theta)\int_0^{\pi/2}\cos^2\theta_{sZ}\theta_{sZ}\exp[-\theta^2_{sZ}/2\sigma^2_\theta]\mathrm{d}\theta_{sZ} \quad (18)$$

Analytical expressions are often desired for numerical simplicity. The integral in eq 18 may be expressed as an infinite series. The squared cosine may first be substituted using standard trigonometry relations:

$$K_{sZ} \cong (1/\sigma^2_\theta)\int_0^{\pi/2}\left[\frac{1}{2}+\frac{1}{2}\cos(2\theta_{sZ})\right]\theta_{sZ}\exp[-\theta^2_{sZ}/2\sigma^2_\theta]\mathrm{d}\theta_{sZ} \quad (19)$$

The cosine term can then be rewritten in the form of an infinite series:

$$K_{sZ} \cong \frac{1}{2}+\frac{1}{2}(1/\sigma^2_\theta)\int_0^{\pi/2}[1+\sum_{n=1}^{\infty}(-1)^n(2\theta_{sZ})^{2n}/(2n)!]\theta_{sZ} \times \exp[-\theta^2_{sZ}/2\sigma^2_\theta]\mathrm{d}\theta_{sZ} \quad (20)$$

Since the integral of a sum is equal to the sum of integrals, eq 20 can be reexpressed as

$$K_{sZ} \cong 1+\frac{1}{2}\sum_{n=1}^{\infty}(-1)^n 2^{2n}/(2n)!(1/\sigma^2_\theta)\int_0^{\pi/2}\theta_{sZ}{}^{2n+1} \times \exp(-\theta^2_{sZ}/2\sigma^2_\theta)\mathrm{d}\theta_{sZ} \quad (21)$$

Assuming that the $\pi/2$ limit in the integral in eq 21 may be replaced by infinity (a very good approximation for values of σ_θ much less than $\pi/2$), each integral in the infinite series is Gaussian in nature and can be explicitly evaluated. Term by term integration followed by simplification yields the following relatively quickly converging series:

$$K_{sZ} \cong 1+\sum_{n=1}^{\infty}(-1)^n[n!/(2n)!]2^{2n-1}(2\sigma^2_\theta)^n \quad (22)$$

Once the value of K_{sZ} has been calculated from roughness measurements, it may be used to isolate the influence of roughness on the local molecular orientation measured by linear dichroism via substitution into eq 12. Specifically, $K_{s\zeta}$ can be determined from knowledge of K_{sZ} and $K_{\zeta Z}$ from linear dichroism measurements. From the value of $K_{s\zeta}$, the mean local molecular tilt angle can be determined for a given distribution function [for a narrow distribution of local molecular tilt angles, $\langle\theta_{s\zeta}\rangle \cong \cos^{-1}(K_{s\zeta}{}^{1/2})$].

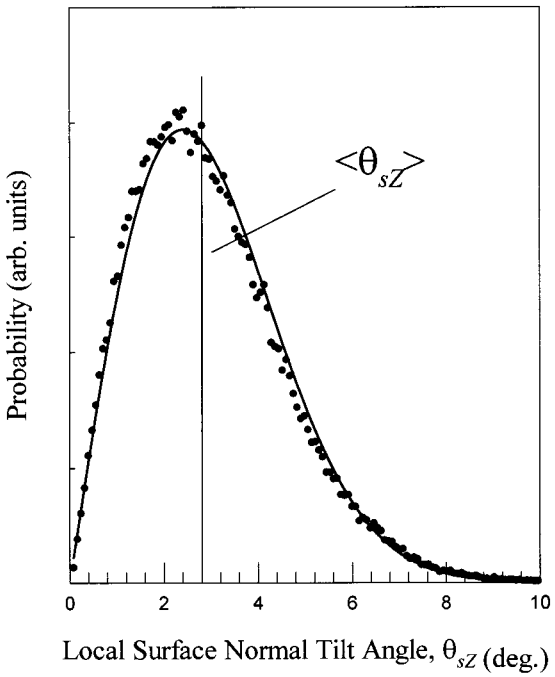

Figure 4. Comparison of the distribution function (given by eq 14) calculated from the distance-dependent roughness (—) with the distribution experimentally measured from analysis of AFM topographs of a silica surface (• • •) . Calculations were performed for a cutoff length equal to 35 nm. The solid vertical line corresponds to the calculated mean of the surface tilt angle distribution (i.e. $\langle\theta_{sZ}\rangle$). The fit yielded a correlation coefficient (R^2) equal to 0.995.

Results and Discussion

The accuracy of the surface tilt distribution proposed in eq 14 is demonstrated in Figure 4, in which an experimentally measured surface tilt distribution (determined from analysis of an AFM image of a mechanically polished fused silica surface) is compared with the predicted distribution. Shown also in Figure 4 is the location of the mean surface tilt angle with respect to the distribution; since the general shape of the distribution changes little with increasing roughness (with the exception of broadening), the mean surface tilt angle can be used as a general parameter to describe the width of the surface tilt angle distribution. In regimes where instrumental artifacts are minimal, the theoretical distribution describes very well the experimentally observed behavior ($R^2 \geq 0.99$).[57] It is reasonable to assume similar correspondence between the theoretical and experimental distributions at essentially any surface with a Gaussian height distribution.

Fractal Analysis of Surface Roughness As Measured by AFM. Despite its use in previous studies, R_q is not an ideal parameter to evaluate the influence of roughness on measured molecular tilt angles for several reasons. Most importantly, R_q values are highly dependent on length scale.[57,59,60] In fact, the exponential dependence of R_q on length scale is well documented and has been used to determine fractal dimensions of surfaces.[59,60] As a result of this dependence, no one AFM scan size can reliably be used to evaluate the roughness. Additionally, AFM roughness measurements of features much smaller than

the tip diameter ($\sim$ 5−40 nm) can be effectively smoothed by tip geometric effects.[61−63] Although multilayer surface films may be of a thickness comparable to the tip diameter, most monolayer and submonolayer surface films are significantly less ($\sim$ 1.5−3 nm) and therefore particularly susceptible to such tip-related artifacts. For these reasons, an alternative method for evaluating the contribution of surface roughness to molecular orientation was developed previously in our laboratory.[57]

In brief, the surface topographs are treated as self-affine fractals in order to extract the distance-dependent variance in height between points separated by distances comparable to the molecular size. Use of the distance-dependent roughness is necessary in order to provide roughness parameters which are independent of image size and to reduce tip-related smoothing effects of features much smaller than the tip diameter ($\sim$10−40 nm). With the probability distribution function calculated using eq 14 or 15, the value of K_{sZ} may be calculated using eq 13.

The fractal analysis approach developed in our laboratory utilizes a well-established variance correlation function of the form[64,65]

$$g_Z(L) = 2\sigma^2_{Z,\infty}[1 - \exp[-(L/\xi)^{2H}]] = \sigma^2_{Z,\text{eff}} \qquad (23)$$

where $g_Z(L)$ is the variance in the difference in heights between points separated by a lateral distance L (as shown in Figure 2), H is a fractal scaling parameter with a value between 0 and 1, ξ is the correlation length, and $\sigma_{Z,\infty}$ is the asymptotic value of R_q evaluated at image sizes much greater than the correlation length. The lateral distance, L, is equal to the cutoff length, since both describe the relevant length scale for surface roughness. Specifically, the cutoff length is equal to the smallest-sized surface feature which can contribute to tilt within the molecular film. It is assumed that features much larger than the molecular size can be treated as locally "flat" with respect to the molecule and that features much smaller than the molecular size do not significantly affect molecular tilt.[57] Together with the exponent H, the correlation length determines the distance required to "lose memory" of an initial height. This loss of memory can be understood if the surface is characterized by relatively large features (e.g. "hills" and "valleys") giving rise to local structure at short distances, which is gradually lost at separations much greater than the feature size. The effective roughness, $\sigma_{Z,\text{eff}}$, introduced in eq 14, is the root-mean-square difference in height evaluated at separations equal to the cutoff length, L, and includes the distance-dependence of the roughness.

Evaluation of *H*. In essence, the variance correlation function given by eq 23 describes the breadth of the height distribution as a function of the separation between points on the surface. The presence of surface structure will reduce the variance measured at separations smaller than the structure size when compared with that measured at much larger separations. In this manner, variance correlation functions provide information about the sizes of structures present on the surface, which is unavailable from standard root-mean-square roughness descriptions (i.e., fractal descriptions can distinguish between a relatively smooth surface with large rolling surface features and a uniformly rough surface, both of which may exhibit an identical root-mean-square roughness). A surface with smooth, rolling features will have a large dependence on scale and a value of H close to 1, while a jagged, fractured surface would be expected to be largely scale-independent with a value of H closer to 0.

The relationship between H and the surface topography is demonstrated further in Figure 5. In this figure, the mean of the local surface normal tilt angle distribution (chosen as a representative value to describe the distribution) is calculated as a function of the asymptotic roughness, $\sigma_{Z,\infty}$. The asymptotic roughness is representative of the root-mean-square roughness, R_q. The mean local surface normal tilt angle was calculated using the distribution given in eq 14 for the effective roughness determined by the variance correlation function given in eq 23. As one can observe in Figure 5, surfaces characterized by rolling features with values of H close to 1 do not produce a highly tilted surface while a jagged surface with H closer to 0 is much more tilted. Clearly, using just root-mean-square roughness analysis will yield an incorrect surface tilt distribution, since it effectively assumes that H is equal to 0.

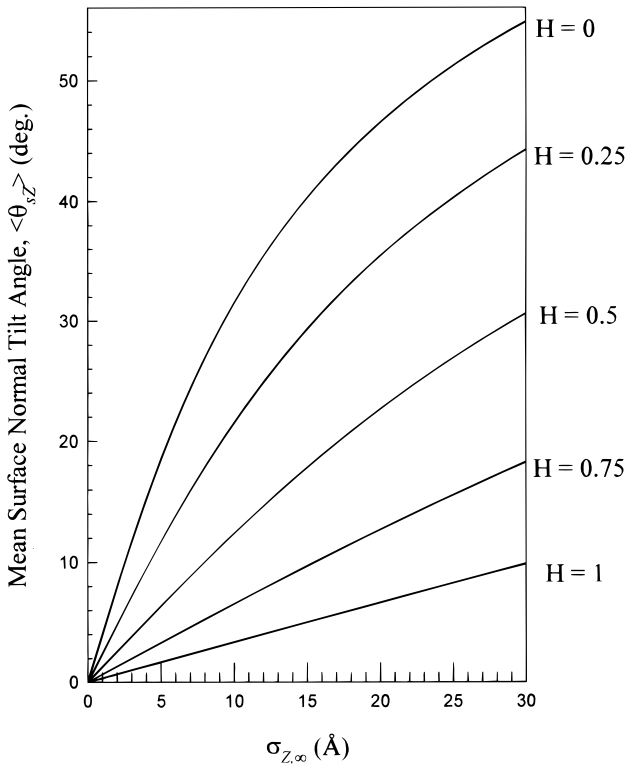

Figure 5. Mean surface tilt angle ($\langle\theta_{sZ}\rangle$) as a function of the asymptotic roughness, $\sigma_{Z,\infty}$, plotted for several different values of H. The mean surface tilt angle (or $\langle\theta_{sZ}\rangle$) is chosen as a representative measure of the breadth of the distribution (see Figure 4) and was calculated using the distribution function given by eq 14. The asymptotic roughness, defined explicitly in eq 24, is related to the root-mean-square surface roughness. A correlation length of 30 nm was chosen arbitrarily for the calculations.

The variance correlation function analysis of a real surface (mechanically polished fused silica) is shown in Figure 6. Specifically, data are shown from fractal analysis of tapping mode AFM micrographs acquired for image sizes ranging from 125 nm × 125 nm to 5 μm × 5 μm. The best-fit curve to eq 23 for the entire data set (given by the solid line) was obtained with H = 0.43, $\sigma_{Z,\infty}$ = 1.35 nm, and ξ = 29.04 nm. By inspection of the data, the variance in height is highly distance-dependent at separations less than $\sim$100 nm but not at larger separations. Qualitatively, this behavior indicates that the surface has features ranging in size up to about 100 nm but relatively few features larger than 100 nm. This finding is certainly reasonable in view of the fact that the surface is optically flat (and therefore void of features comparable in size to the wavelength of light) but mechanically polished. For mechanically polished surfaces such as fused silica, fractal scaling behavior is common, with the correlation length, ξ, expected to be on the order of the polishing grit size.[66]

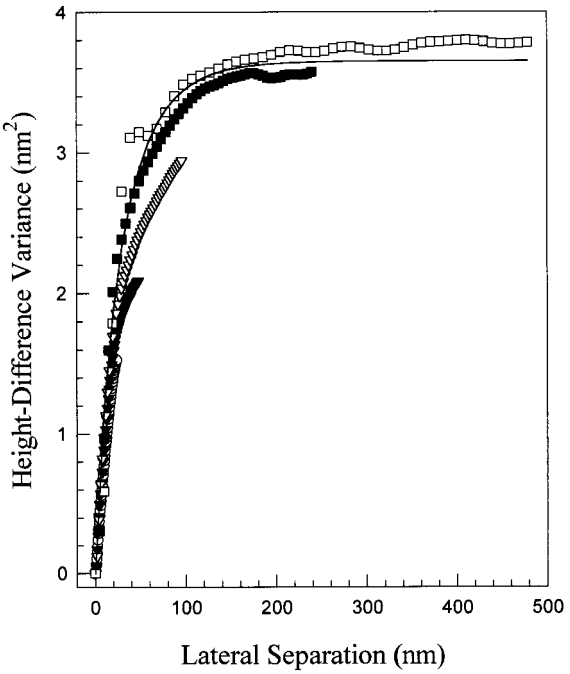

Figure 6. Variance correlation function analysis from AFM micrographs of a fused silica surface. The scan size was varied from 125 nm to 5 μm: (●) 125 nm, (○) 250 nm, (▲) 500 nm, (△) 1 mm, (■) 2.5 μm, (□) 5 μm. The solid line represents a best fit, yielding the fractal parameters $H = 0.43$ ($\pm$ 0.02), $\sigma_{Z,\infty} = 1.35$ nm ($\pm$ 0.02 nm), and $\xi = 29.04$ nm ($\pm$ 0.02 nm). Figure adapted from ref 57.

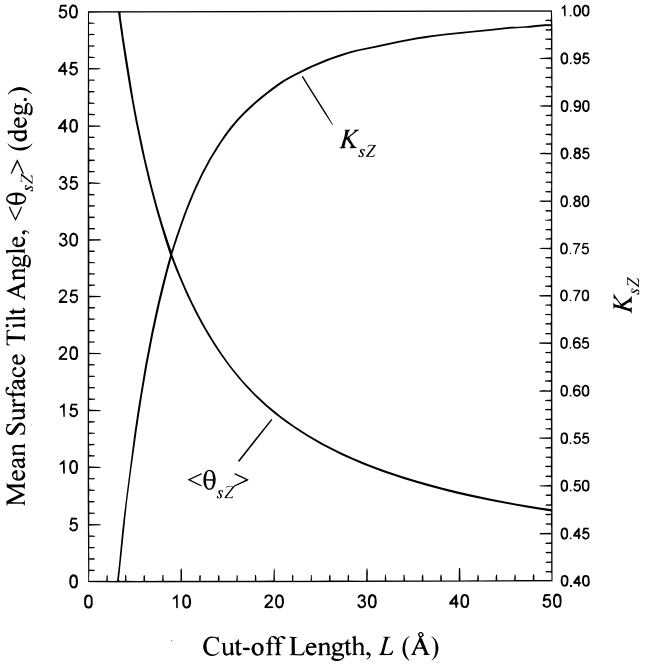

Figure 7. Using the experimental fractal fitting parameters acquired from AFM micrographs of fused silica (see Figure 6), both K_{sZ} and the mean surface tilt angle (see Figure 4) are calculated as functions of the cutoff length for a fused silica surface.

Evaluation of *L*. By inspection of both the distribution function given in eq 14 and the variance correlation function in eq 23, it is observed that the local surface normal tilt angle distribution is doubly dependent on the value of the cutoff length. In the first case, reduction in the cutoff length leads to an increase in the surface tilt angle, since the tilt is calculated from $\Delta Z/L$. However, in the second case, reduction in the cutoff length leads to a reduction in the effective roughness for cutoff lengths smaller than the correlation length. The interplay between these two competing influences is illustrated in Figure 7, in which both K_{sZ} and $\langle\theta_{sZ}\rangle$ (calculated using eq 16 and from the mean of the distribution given by eq 14) are shown as functions of the cutoff length using the variance correlation function parameters obtained for a fused silica surface. It is clear from the figure that for the smaller cutoff lengths ($L < 20$ Å), the tilt angle distribution is highly dependent on the cutoff length. However, for cutoff lengths greater than ~25 Å, both K_{sZ} and $\langle\theta_{sZ}\rangle$ are relatively insensitive to changes in the cutoff length, which suggests that, at these length scales, the surface tilt angle distribution is dominated by the tilt due to features significantly larger than the cutoff length. In the limit of an asymptotically large cutoff length, the mean surface tilt approaches 0 and K_{sZ} approaches 1, in agreement with the notion that the surface is flat on size scales at least as large as the wavelength of light.

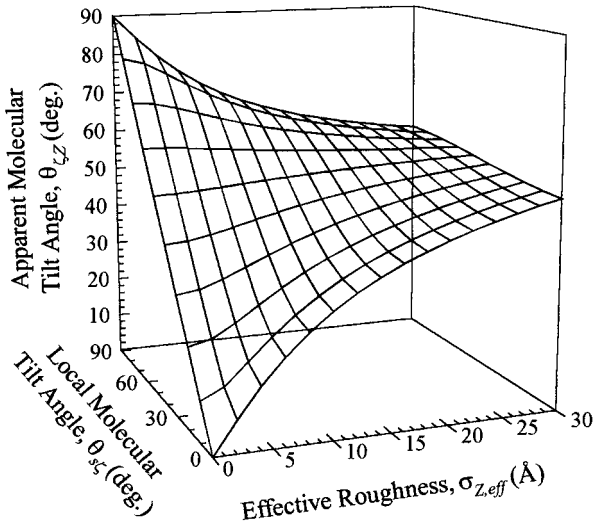

Figure 8. Effect of increasing roughness on the apparent molecular orientation angle ($\theta_{\zeta Z}$*), as measured by linear dichroism, is shown as a function of both the local molecular orientation angle ($\theta_{s\zeta}$) and the effective substrate roughness ($\sigma_{Z,\text{eff}}$). The asterisk indicates that $\theta_{\zeta Z}$* was calculated by assuming (incorrectly in this case) a δ-function molecular distribution, thereby neglecting surface roughness effects in the calculations. A cutoff length of 20 Å was assumed in the calculations. It should be noted that the magic angle is not a true asymptote of the distribution given by eq 14. At large values of the effective roughness, the calculated curves do not converge to the magic angle result due to the failure of treating the surface as a single-valued function (i.e., with no overhanging features). This approximation is necessary to allow for fractal roughness analysis, without which the mathematics become intractable. However, reasonable surfaces for which the topography may be reliably measured from AFM imaging will necessarily be well-described by single-valued functions and therefore amenable to the analysis described in this paper.

The reliability of the proposed method for quantifying roughness effects on molecular orientation measurements depends on both the quality of the theoretical treatment and the accuracy of the roughness measurements. The conditions under which AFM provides quantitative roughness measurements[67−70] was the subject of a previous study in our laboratory.[34] All of the AFM data discussed in this paper were acquired under the appropriate conditions. Additionally, we have also previously confirmed that AFM micrographs can be used to reliably determine the local surface normal tilt angle distribution at molecular scales.[57]

Application of Theory. Figure 8 shows the apparent molecular tilt angle ($\theta_{\zeta Z}$*) as a function of both the local molecular tilt angle ($\theta_{\zeta Z}$) and the effective surface roughness ($\sigma_{Z,\text{eff}}$). The

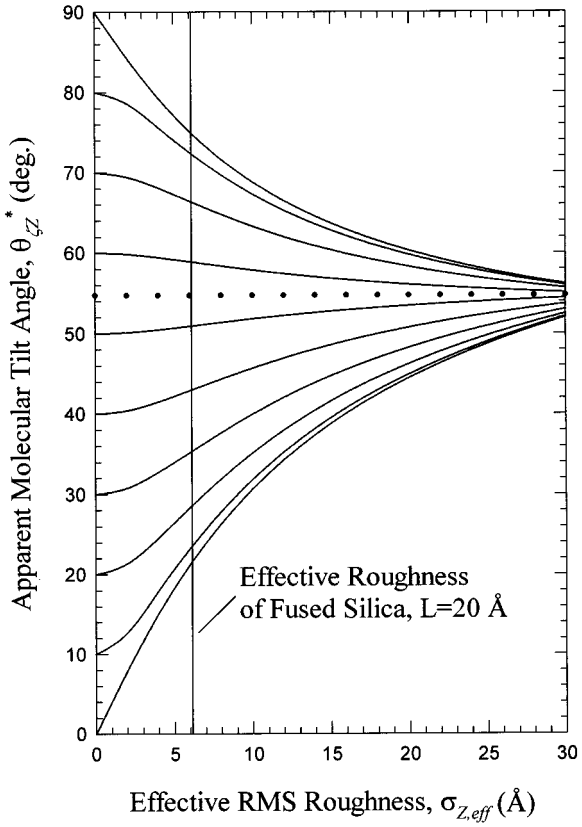

Figure 9. The apparent tilt angle, $\theta_{\zeta Z}$*, is plotted as a function of the effective surface roughness for a cutoff length of 20 Å. Each curve corresponds to a different local molecular orientation angle, $\theta_{s\zeta}$, given as the *y* intercept (i.e., the tilt observed for a perfectly smooth surface). For example, the second curve from the bottom corresponds to a local tilt angle of 10°. The solid vertical line corresponds with the effective roughness measured for fused silica at a cutoff length of 20 Å.

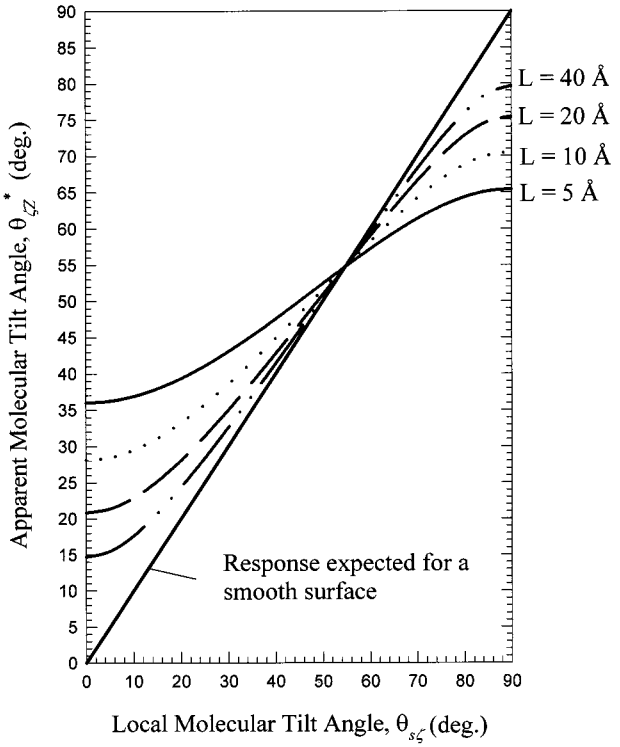

Figure 10. Using the experimental roughness measurements shown in Figure 6 for a fused silica surface, the apparent molecular tilt angle, $\theta_{\zeta Z}$* (see eq 6), is plotted as a function of the local molecular tilt angle, $\theta_{s\zeta}$, for a variety of cutoff lengths. The error introduced by neglect of surface roughness in the interpretation of linear dichroism measurements is the difference between the calculated curves and the straight line, corresponding to the smooth surface response. For example, neglect of surface roughness at a cutoff length of 20 Å and a local molecular tilt angle of 0° yields an error of ~21° in the interpretation of the linear dichroism orientation measurements.

apparent molecular tilt angle, as defined in eq 6, is the value most often reported as the average molecular tilt angle for linear dichroism based measurements at surfaces. For clarity in these calculations, the local molecular tilt angle is assumed to be a constant (In fact, any distribution function is valid provided that $\theta_{s\zeta}$ is equal to $\cos^{-1}(K_{s\zeta}^{1/2})$. For the cases of $\theta_{s\zeta} =$ (0° and 90°, only the δ function satisfies this condition) (i.e., the local molecular tilt angle distribution is assumed to be a δ function centered at $\theta_{s\zeta}$). As observed in Figure 8, for an effective roughness of 0, the local molecular tilt angle is identical to the macroscopic tilt angle, as expected. As the effective roughness increases, the macroscopic tilt angle approaches the magic angle result of 54.7° (i.e., the result obtained for an unoriented system), regardless of the local molecular orientation.

The quantitative relationship between the apparent macroscopic tilt angle, $\theta_{\zeta Z}$*, and the effective roughness is more clearly observable in Figure 9, in which the apparent molecular tilt angle is shown as a function of the effective roughness for several different local surface tilt angles. Included in Figure 9 is the effective roughness of fused silica calculated from fractal analysis of AFM images. The intercept of each curve ($\sigma_{Z,\mathrm{eff}} =$ 0) corresponds to the tilt observed at a perfectly smooth surface and yields the value of the local molecular tilt angle (e.g., for the second curve from the bottom, $\theta_{s\zeta} = 10°$). As shown in the figure, the roughness present on fused silica surfaces is great enough to introduce large differences between the local molecular tilt angle and the macroscopically observed tilt angle. For example, if it is incorrectly assumed that the apparent macroscopic molecular tilt angle is equal to the local molecular tilt angle, roughness can introduce errors as large as 21° in the interpretation of linear dichroism orientation measurements for a molecular size of 20 Å at fused silica surfaces.

The error introduced by neglect of roughness is further clarified in Figure 10, in which the apparent macroscopic molecular tilt angle is calculated as a function of the local molecular tilt angle using the variance correlation function parameters determined from experimental data for fused silica (Figure 6). Calculations were performed for several different cutoff lengths. For each curve, the error introduced by surface roughness is the difference between the apparent macroscopic tilt angle and the local molecular tilt angle and is the difference between each calculated curve and the straight line result for a smooth surface. The curve calculated for a cutoff length of 20 Å corresponds to the vertical line depicted in Figure 9. Note that the error increases with smaller molecular size (i.e., cutoff length). This dependence on cutoff length can be easily understood by reasoning that the orientation of smaller molecules is affected by a greater number of roughness features. A local molecular tilt angle of 54.7° (the magic angle) is a special case; no error is introduced by surface roughness at that particular molecular tilt angle, and the error increases progressively as the tilt angle varies from the magic angle. This particular case is exactly analogous to the instance described earlier in which an infinitely rough surface yields an apparent macroscopic tilt angle of 54.7° regardless of the local molecular tilt angle. From eq 12, if either K_{sZ} (due to surface roughness) or $K_{s\zeta}$ (due to local orientation) is equal to 1/3, then $K_{\zeta Z}$ will be equal to 1/3, yielding a macroscopic tilt angle of 54.7°.

TABLE 1: Molecular Orientation of Azo-Dye Chromophore as a Function of the Number of Layers[a]

layers	$\theta_{\zeta Z}$*[a]	$\theta_{s\zeta}$[a]	$\theta_{\zeta Z}$*[b]	$\theta_{s\zeta}$[b]
1	32°	31°	49°	47°
2	24°	23°	38°	33°
3	19°	18°	27°	25°
4	24°	23°	38°	34°
5	14°	13°	20°	18°
6	15°	14°	22°	20°

[a] Data adapted from ref 29. The angle $\theta_{\zeta Z}$* is the apparent molecular tilt angle neglecting surface roughness, and $\theta_{s\zeta}$ is the local molecular tilt angle corrected for surface roughness. The superscript a indicates a molecular tilt angle calculated assuming no rotation about the long molecular axis ($\theta_{s\zeta} = 90° - \theta_{fs}$). The superscript b indicates molecular tilt angle calculated assuming free rotation about the long molecular axis (using eq A8).

Consequently, if either the surface molecules are all oriented locally at 54.7° or if they are completely unoriented (it is impossible to distinguish between the two cases using linear dichroism on a single transition), the apparent macroscopic tilt angle will not change from the magic angle as the roughness is increased. Again, this result is intuitively appealing, since a sample which does not exhibit linear dichroism at a smooth surface should not do so at a rough one.

The approach of the apparent macroscopic tilt angle to 54.7°, apparent in both Figures 8 and 9, is particularly significant. As mentioned previously, if K_{sZ} has a value of 1/3, corresponding to an equal probability of all surface tilt angles [$1/3 = \cos^2(54.7°)$], the value of $K_{\zeta Z}$ will also equal 1/3 regardless of the value of $K_{s\zeta}$. In other words, an infinitely rough surface should yield a molecular tilt angle equal to the magic angle and consequently provide no information about the local molecular tilt angle. The fact that the distribution function proposed in eq 14 yields calculated macroscopic tilt angles which converge to the magic angle provides evidence that the proposed distribution is physically reasonable.

Reevaluation of Published Results. Using the method proposed in this paper, previously reported ARPAS results were reexamined in order to correct for the influence of surface roughness on the orientation measured in multilayer azo-dye films.[33] Previously published and corrected data are shown in Table 1. In the ARPAS investigation, the short axis transition moment of the azo dye was probed. Two possibilities for the molecular orientation were calculated from the experimental value of K_{fZ}: one in which the molecular rotation about the long axis is restricted (such that $\theta_{s\zeta}$ equals $90° - \theta_{fs}$) and the second in which free rotation about the long molecular axis is assumed (such that $\theta_{s\zeta}$ is calculated using eq A8). While it is unknown which of these two cases is more representative of the true molecular tilt angle, the trend with the number of layers is the same in each case—increased alignment with the surface normal with increased number of layers. We have attributed the trend to improved packing in lower layers upon deposition of additional layers.[33] Most notable in Table 1 is the fact that the correction for surface roughness is never more than 5°. Recall that the worst-case scenario for a molecule of this size (20 Å) is an error as great as 21° (see Figure 10). For the first layer, the small error can be easily explained by noting that the short axis, which contains the transition moment, is tilted close to the magic angle (θ_{fZ}* = 58° ≈ 54.7°). As shown in Figure 10, the error in neglecting roughness for tilt angles close to the magic angle is relatively small, in this case not more than a couple of degrees. However, as the number of layers increases, the error does not change much although the film changes both in thickness and in the molecular orientation angle. This fact is somewhat unexpected. Increasing the cutoff length by the addition of layers should lead to a decrease in the error associated with surface roughness (see Figure 7). In contrast, as the long axis of the molecule tilts more toward the surface normal (and correspondingly as the short axis tilts further away from the magic angle), an increase in the error in the local molecular tilt angle is expected (see Figure 10). The remarkable uniformity of the roughness correction can therefore be attributed to the coincidental competition between an increase in cutoff length and an increase in molecular alignment toward the local surface normal as the number of layers is increased. Another significant finding is that roughness can still influence the measured tilt angle even at cutoff lengths greater than the root-mean-square roughness ($L = 40-120$ Å compared with an R_q of 13.5 Å for fused silica), in contrast to previous expectations.[39,55]

Summary and Future Directions. The combined results of this analysis provide a simple, universal method for correction of surface roughness effects on molecular orientation measurements made by linear dichroism. The general approach is (1) the effective surface roughness is first determined by fractal analysis of AFM micrographs, (2) using the effective roughness in the probability distribution given by eq 14, the value of K_{sZ} is calculated, (3) the value of $K_{\zeta Z}$ is determined from linear dichroism measurements, and (4) $K_{s\zeta}$, which is effectively the corrected linear dichroism result, is calculated from the known values of K_{sZ} and $K_{\zeta Z}$ using the relation given in eq 12. The corrected measurement of molecular orientation with respect to the local surface should provide a better understanding of thin film−surface interactions.

Since the mathematical relations in this paper are quite general, the theory can easily be extended to orientation measurements other than linear dichroism. For example, the same general treatment of a distribution in molecular orientation recently led us to postulate the existence of a "magic angle" in second-harmonic generation.[71] In this case, as the distribution broadens, the measured orientation angles converge to 39.2°. Thus, it is clear that quantitative consideration of the influence of surface roughness will lead to new insight into molecular orientation and its measurement.

Acknowledgment. The authors gratefully acknowledge funding from the National Science Foundation.

Appendix: Off-Axis Transition Moments

If the transition moment does not lie along the molecular orientation axis, then the angle between the transition moment and the local surface normal (i.e., θ_{fs}) is no longer equal to the angle between the molecular axis and the surface normal (i.e., $\theta_{s\zeta}$). Consequently, a more general form for eq 12 must be used

$$K_{fZ} = \frac{1}{2}[1 - K_{sZ} - K_{fs} + 3K_{sZ}K_{fs}] \quad \text{(A1)}$$

where K_{fs} refers to the angle between the transition moment and the local surface normal, θ_{fs}. By analogy with the derivation of eq 9

$$K_{fs} = K_{s\xi}\cos^2\theta_{f\xi} + K_{s\Psi}\cos^2\theta_{f\Psi} = K_{s\zeta}\cos^2\theta_{f\zeta} \quad \text{(A2)}$$

If it is assumed that there is free rotation about the molecular orientation axis, then

$$K_{s\xi} = K_{s\psi} = \frac{1}{2}(1 - K_{s\zeta}) \quad \text{(A3)}$$

Substitution into eq A2 yields

$$K_{fs} = \frac{1}{2}(1 - K_{s\xi})(\cos^2 \theta_{f\xi} + \cos^2 \theta_{f\Psi}) + K_{s\zeta} \cos^2 \theta_{f\zeta} \quad \text{(A4)}$$

$$K_{fs} = \frac{1}{2}[\sin^2 \theta_{f\zeta} - K_{s\xi} \sin^2 \theta_{f\zeta} + 2K_{s\zeta} \cos^2 \theta_{f\zeta}] \quad \text{(A5)}$$

$$K_{fs} = \frac{1}{2}[\sin^2 \theta_{f\zeta} - K_{s\zeta}(3 \sin^2 \theta_{f\zeta} - 2)] \quad \text{(A6)}$$

Notice that in the limit of the transition moment lying along the orientation axis, then $K_{fs} = K_{fZ}$ and eq 12 is regenerated. If the transition moment lies along either the molecular ξ or ψ axes, then

$$K_{fs} = \frac{1}{2}(1 - K_{s\zeta}) \quad \text{(A7)}$$

$$K_{fZ} = \frac{1}{4}(1 + K_{sZ} + K_{s\zeta} - 3K_{sZ}K_{s\zeta}) \quad \text{(A8)}$$

Equation A8 differs from eq 12 by a factor of 1/4 (rather than 1/2) and by a sign change.

In more general cases in which the angle between the transition moment and the molecular orientation axis is neither 0° nor 90°, eq A3 may be used to calculate the value of $K_{s\zeta}$ (related to the local orientation) from the value of K_{fs}. Determination of K_{fs} can be achieved after removing the roughness contributions from the experimentally obtained value of K_{fZ} (eq A1). Putting everything together

$$K_{fZ} = \frac{1}{2}\Big(1 - K_{sZ} - \frac{1}{2}[\sin^2 \theta_{f\zeta} - K_{s\zeta}(3 \sin^2 \theta_{f\zeta} - 2)] + K_{sZ}\frac{3}{2}[\sin^2 \theta_{f\zeta} - K_{s\zeta}(3 \sin^2 \theta_{f\zeta} - 2)]\Big) \quad \text{(A9)}$$

where

$$K_{sZ} = N_{2D}\int_0^{\pi/2}(\cos^2 \theta_{sZ})\theta_{sZ} \sec^2 \theta_{sZ} \times \exp[-(L \tan \theta_{sZ})^2/2\sigma^2_{Z,\text{eff}}]d\theta_{sZ} \quad \text{(A10)}$$

and

$$\sigma^2_{Z,\text{eff}} = 2[\sigma_{Z,\infty} - \exp(-(L/\xi)^{2H})] \quad \text{(A11)}$$

References and Notes

(1) For example, see: (a) Enderle, Th.; Meixner, A. J.; Zschokke-Gränacher *J. Chem. Phys.* **1994**, *101*, 4365. (b) Lehmann, S.; Busse, G.; Kahlweit, M.; Stolle, R.; Simon, F.; Marowsky, G. *Langmuir* **1995**, *11*, 1174. (c) Zhang, D.; Gutow, J.; Eisenthal, K. B. *J. Phys. Chem.* **1994**, *98*, 13729. (d) Zhang, T.; Feng, Z.; Wong, G. K.; Ketterson, J. B. *Langmuir* **1996**, *12*, 2298. (e) Zhao, X.; Eisenthal, K. B. *J. Chem. Phys.* **1995**, *102*, 5818.

(2) (a) Shen, Y. R. *Annu. Rev. Phys. Chem.* **1989**, *40*, 327. (b) McGilp, J. F. *Appl. Surf. Sci.* **1993**, *63*, 99. (c) Bohn, P. W. *Annu. Rev. Meter. Sci.* **1997**, *27*, 469. (d) Bohn, P. W.; Walls, D. J. *Mikrochim. Acta* **1991**, *I*, 3.

(3) (a) Gragson, D. E.; Richmond, G. L. *Langmuir* **1997**, *13*, 4804. (b) Baldelli, S.; Schnitzer, C.; Shultz, M. J.; Campbell, D. J. *J. Phys. Chem. B* **1997**, *101*, 4607.

(4) Zyss, J. *Molecular Nonlinear Optics*; Academic Press: San Diego, CA, 1994.

(5) Kajzar, F.; Swalen, J. D. *Organic Thin Films for Waveguiding Nonlinear Optics*; Overseas Publishers Association: Amsterdam, 1996.

(6) Ulman, A. *An Introduction to Ultrathin Organic Films; From Langmuir−Blodgett to Self- Assembly*; Academic Press: New York, 1991; pp 242, 251.

(7) Rutan, S. C.; Harris, J. M. *J. Chromatogr.* **1993**, *656*, 197.

(8) Edmiston, P. L.; Lee, J. E.; Wood, L. L.; Saavedra, S. S. *J. Phys. Chem.* **1996**, *100*, 775.

(9) Thompson, N. L.; McConnell, H. M.; Burghardt, T. P. *Biophys. J.* **1984**, *46*, 739.

(10) Parry, D. B.; Harris, J. M. *Appl. Spectrosc.* **1988**, *42*, 997.

(11) Wirth, M. J.; Burbage, J. D. *J. Phys. Chem.* **1992**, *96*, 9022.

(12) Umemura, J.; Kamata, T.; Kawai, T.; Takenaka, T. *J. Phys. Chem.* **1990**, *94*, 62.

(13) Lakowicz, J. R.; Gryczynski, I.; Gryczynski, Z.; Danielsen, E.; Wirth, M. J. *J. Phys. Chem.* **1992**, *96*, 3000.

(14) Wirth, M. J.; Chou, S. H.; Piasecki, D. A. *Anal. Chem.* **1991**, *63*, 146.

(15) Saavedra, S. S.; Reichert, W. M. *Langmuir* **1991**, *7*, 995.

(16) Heinz, T. F.; Tom, H. W. K.; Shen, Y. R. *Phys. Rev. A* **1983**, *28*, 1883.

(17) Shen, Y. R. *Annu. Rev. Phys. Chem.* **1989**, *40*, 327.

(18) Shen, Y. R. *Chemistry and Structure at Interfaces: New Laser and Optical Techniques;* Hall, R. B., Ellis, A. B., Eds.; VCH Publishers Inc.: Deerfield Beach, FL, 1986; Chapter 4.

(19) Dick, B.; Gierulski, A.; Marowsky, G.; Reider, G. A. *Appl. Phys. B* **1985**, *38*, 107. Guyot-Sionnest, P.; Shen, Y. R.; Heinz, T. F. *Appl. Phys. B* **1987**, *42*, 237.

(20) Buck, M. *Appl. Phys. A* **1992**, *55*, 395.

(21) Lin, S. H.; Hayashi, M.; Lin, C. H.; Yu, J.; Villaeys, A. A.; Wu, G. Y. C. *Mol. Phys.* **1995**, *84*, 453.

(22) Gragson, D. E.; McCarty, B. M.; Richmond, G. L. *J. Am. Chem. Soc.* **1997**, *119*, 6144.

(23) Huston, A. L.; Reimann, C. T. *Chem. Phys.* **1991**, *149*, 401.

(24) deMello, A. J.; Elliott, J. A.; Rumbles, G. *J. Chem. Soc., Faraday Trans.* **1997**, *23*, 4723.

(25) Arias, J.; Aravind, P. K.; Metiu, H. *Chem. Phys. Lett.* **1982**, *85*, 404.

(26) Cnossen, G.; Drabe, K. E.; Wiersma, D. A. *J. Chem. Phys.* **1993**, *7*, 5276.

(27) Hirose, C.; Akamatsu, N.; Domen, K. *Appl. Spectrosc.* **1992**, *46*, 1051.

(28) Doughty, S. K.; Rowlen, K. L. *J. Phys. Chem.* **1995**, *99*, 2143.

(29) Montgomery, M. E.; Green, M. A.; Wirth, M. J. *Anal. Chem.* **1992**, *64*, 1170.

(30) Montgomery, M. E.; Wirth, M. J. *Anal. Chem.* **1994**, *66*, 680.

(31) Cropek, C. M.; Bohn, P. W. *J. Phys. Chem.* **1990**, *94*, 6452.

(32) Slotfeldt-Ellingsen, D.; Resing, H. A. *J. Phys. Chem.* **1980**, *84*, 2204.

(33) Doughty, S. K.; Simpson, G. J.; Rowlen, K. L. *J. Am. Chem. Soc.* **1998**, *120*, 7997.

(34) Simpson, G. J.; Sedin, D. L.; Rowlen, K. L. *Langmuir* **1999**, *15*, 1429.

(35) Ulman, A. *Thin Solid Films* **1996**, *273*, 48−53.

(36) Eick, J. D.; Good, R. J.; Neumann, A. W. *J. Colloid Interface Sci.* **1975**, *53*, 23.

(37) Blacke, W. L.; Leung, P. T. *Phys. Rev. B* **1997**, *56*, 12625.

(38) Arias, J.; Aravind, P. K.; Metiu, H. *Chem. Phys. Lett.* **1982**, *85*, 404.

(39) Piasecki, D. A.; Wirth, M. J. *Langmuir* **1994**, *10*, 1913.

(40) Piasecki, D. A.; Wirth, M. J. *J. Phys. Chem.* **1993**, *97*, 7700.

(41) Wirth, M. J.; Burbage, J. D. *J. Phys. Chem.* **1992**, *96*, 9022.

(42) Burbage, J. D.; Wirth, M. J. *J. Phys. Chem.* **1992**, *96*, 5943.

(43) Stuchebryukov, S. D.; Rudoy, V. M. *Vib. Spectrosc.* **1992**, *4*, 95.

(44) Creager, S. E.; Hockett, L. A.; Rowe, G. K. *Langmuir* **1992**, *8*, 854.

(45) Guo, L.; Facci, J. S.; McLendon, G.; Mosher, R. *Langmuir* **1994**, *10*, 4588.

(46) Lu, J. R.; Simister, E. A.; Thomas, R. K.; Penfold, J. *J. Phys., Condens. Matter* **1994**, *9*, A403.

(47) Lu, J. R.; Li, Z. X.; Thomas, R. K. *J. Phys. Chem.* **1993**, *97*, 8012.

(48) Li, Z. X.; Thomas, R. K.; Rennie, A. R.; Penfold, J. *J. Phys. Chem. B* **1998**, *102*, 185.

(49) Bennaatar, J. J.; Daillant, J. *Phase Transitions* **1991**, *30*, 79.

(50) Logothetidis, S.; Sterfidoudis, G. *Appl. Phys. Lett.* **1997**, *71*, 2463.

(51) Lee, C.-H.; Tseng, S.-Y. *J. Appl. Crystallogr.* **1998**, *31*, 181.

(52) Tsuji, K.; Sasaki, A.; Hirokawa, K. *Jpn. J. Appl. Phys.* **1994**, *33*, 6316.

(53) Tsuji, K.; Yamada, T. Utaka, T.; Hirokawa, K. *J. Appl. Phys.* **1995**, *78*, 969.

(54) Ramsey, D. A.; Ludema, K. C. *Rev. Sci. Instrum.* **1994**, *65*, 2874.

(55) Firestone, M. A.; Shank, M. L.; Sligar, S. G.; Bohn, P. W. *J. Am. Chem. Soc.* **1996**, *118*, 9033.

(56) Michl, J.; Thulstrup, E. K. *Spectroscopy with Polarized Light; Solute Alignment by Photoselection, in Liquid Chrystals, Polyners, and Membranes*; VCH Publishers: New York, 1995; Chapter 5.

(57) Simpson, G. J.; Rowlen, K. L. *J. Phys. Chem. B* **1999**, *103*, 1525.

(58) Atkins, P. W. *Physical Chemistry*, 4th ed.; W. H. Freeman and Co.: New York, 1990; Chapter 24.

(59) Williams, J. M.; Beebe, T. P. *J. Phys. Chem.* **1993**, *97*, 6249.

(60) Williams, J. M.; Beebe, T. P. *J. Phys. Chem.* **1993**, *97*, 6255.

(61) Westra, K. L.; Thomson, D. J. *J. Vac. Sci. Technol. B.* **1995**, *13*, 344.

(62) Villarrubia, J. S. *Surf. Sci.* **1994**, *321*, 287.

(63) Reiss, G.; Vancea, J.; Wittmann, H.; Zweck, J.; Hoffmann, H. *J. Appl. Phys.* **1990**, *67*, 1156.

(64) Palasantzas, G. *Phys. Rev. B.* **1993**, *48*, 14472.

(65) Pynn, R. *Phys. Rev. B.* **1992**, *45*, 602.

(66) Bennett, J. M.; Mattson, L. *Introduction of Surface Roughness and Scattering;* Optical Society of America: Washington, DC, 1989; Chapter 4.

(67) Munkholm, A.; Brennan, S.; Carr, E. C. *J. Appl. Phys.* **1997**, *82*, 2944.

(68) Chu, P. K.; Brigham, R. G.; Baumann, S. M. *Mater. Chem. Phys.* **1995**, *41*, 61.

(69) Abe, T.; Steigmeier, E. F.; Hagleitner, W.; Pidduck, A. J. *Jpn. J. Appl. Phys.* **1992**, *31*, 721.

(70) Dumas, P.; Bouffakhreddine, B.; Amra, C.; Vatel, O.; Andre, E.; Galindo, R.; Salvan, F. *Europhys. Lett.* **1993**, *22*, 717.

(71) Simpson, G. J.; Rowlen, K. L. *J. Am. Chem. Soc.*, in press.